Comparison of a Brush-with-Anchor and a Train-of-Brushes Mucin on Poly(methyl methacrylate) Surfaces: Adsorption, Surface Forces, and Friction

ARTICLE *in* BIOMACROMOLECULES · MARCH 2014

Impact Factor: 5.75 · DOI: 10.1021/bm500173s · Source: PubMed

Biomacromolecules

Article

pubs.acs.org/Biomac

Comparison of a Brush-with-Anchor and a Train-of-Brushes Mucin on Poly(methyl methacrylate) Surfaces: Adsorption, Surface Forces, and Friction

Junxue An,[†] Andra Dėdinaitė,*[,†,‡] Anki Nilsson,[§] Jan Holgersson,[∥] and Per M. Claesson[†,‡]

[†]School of Chemical Science and Engineering, Department of Chemistry, Division of Surface and Corrosion Science, KTH Royal Institute of Technology, Drottning Kristinas väg 51, SE-100 44 Stockholm, Sweden

[‡]Chemistry, Materials and Surfaces, SP Technical Research Institute of Sweden, P. O. Box 5607, SE-114 86 Stockholm, Sweden

[§]Recopharma AB, Arvid Wallgrens backe 20, 413 46 Gothenburg, Sweden

[∥]Department of Clinical Chemistry and Transfusion Medicine, The Sahlgrenska Academy, University of Gothenburg and Sahlgrenska University Hospital, Vita stråket 13, SE-413 45 Gothenburg, Sweden

Supporting Information

ABSTRACT: Interfacial properties of two types of mucins have been investigated at the aqueous solution/poly(methyl methacrylate) (PMMA) interface. One is commercially available bovine submaxillary mucin, BSM, which consists of alternating glycosylated and non-glycosylated regions. The other one is a recombinant mucin-type fusion protein, PSGL-1/mIgG$_{2b}$, consisting of a glycosylated mucin part fused to the Fc part of an immunoglobulin. PSGL-1/mIgG$_{2b}$ is mainly expressed as a dimer upon production. A quartz crystal microbalance with dissipation was used to study the adsorption of the mucins to PMMA surfaces. The mass of the adsorbed mucin layers, including the adsorbed mucin and water trapped in the layer, was found to be significantly higher for PSGL-1/mIgG$_{2b}$ than for BSM. Atomic force microscopy with colloidal probe was employed to study interactions and frictional forces between mucin-coated PMMA surfaces. Purely repulsive forces of steric origin were observed between PSGL-1/mIgG$_{2b}$ mucin layers, whereas a small adhesion was detected between BSM layers and attributed to bridging. Both mucin layers reduced the friction force between PMMA surfaces in aqueous solution. The reduction was, however, significantly more pronounced for PSGL-1/mIgG$_{2b}$. The effective friction coefficient between PSGL-1/mIgG$_{2b}$-coated PMMA surfaces is as low as 0.02 at low loads, increasing to 0.24 at the highest load explored, 50 nN. In contrast, a friction coefficient of around 0.7 was obtained between BSM-coated PMMA surfaces. The large differences in interfacial properties for the two mucins are discussed in relation to their structural differences.

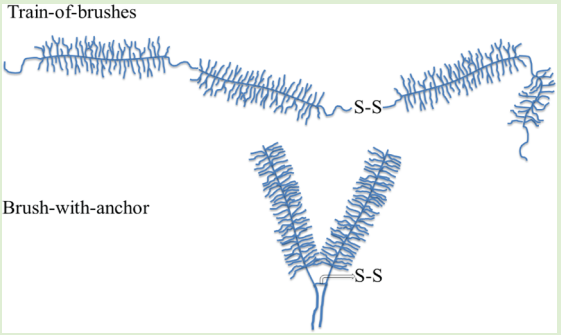

1. INTRODUCTION

Mucins constitute a large family of glycoproteins with high molecular weight ranging from 0.5 to 40 MDa.[1] They exist in secreted and membrane-bound forms and coat almost all wet surfaces in the mammalian body,[2] for example the eye[3,4] and oral surfaces.[5] It is generally accepted that mucin-type glycoproteins together with other components in mucus provide protective and lubricating properties. In addition, mucin-coated surfaces have nonadhesive properties, which mean that they can prevent other proteins and bacteria from adsorbing to, e.g., biomedical implants.[6,7] Although different mucin types have various size, carbohydrate content, charge density, and overall structure, they share certain common features. The subunits of mucins consist of a polypeptide main chain, which contains heavily glycosylated domains separated by short nonglycosylated or sparsely glycosylated patches, known as "naked" regions. The glycosylated domains are rich in serine and threonine residues, which are anchoring points for O-linked oligosaccharide side chains. The oligosaccharides constitute 50−80% of the dry weight of mucin molecules,[2,8] and they provide strong interactions with water.[9] The presence of sialic acid and sulfate ester residues gives most mucins an overall negative charge.[2] Secreted mucins can contain cysteine rich domains that facilitate self-association via cysteine−cysteine interactions and are hence gel-forming.[2,8,10]

Mucins can adsorb to a wide range of surfaces by hydrogen bonding,[11,12] hydrophobic,[6,7,13] and electrostatic interactions.[14] The adsorption of mucin on different hydrophobic surfaces, polystyrene,[6,13,15] hydrophobized silica and mica,[14,16,17] and poly(methyl methacrylate) (PMMA)[11,18] has been studied by different techniques. Previous studies showed that mucins adsorb more on hydrophobic surfaces than on hydrophilic ones, and with negligible desorption upon rinsing.[14,16,19] For instance, Cardenas et al. studied adsorption of a salivary mucin,

Received: February 3, 2014
Revised: March 20, 2014
Published: March 21, 2014

MUC5B, on both hydrophilic and hydrophobized silica with ellipsometry. It was found that the adsorbed amount was much larger on the hydrophobic substrate (2.4 mg/m^2) than on the hydrophilic one (0.5 mg/m^2).[5] It was suggested that the nonglycosylated regions facilitate attachment to the hydrophobic surface via hydrophobic forces, whereas the highly hydrated oligosaccharide side chains stretch away from the main chain, resulting in a "bottle-brush" configuration.[20] This is expected to provide good wettability due to the water retention ability of the oligosaccharides.[13] Moreover, this configuration can also provide good lubrication properties as a result of steric and electrostatic repulsion.[6,7,13,21]

The lubrication ability of mucins *in vivo* can be ascribed to two aspects. In the bulk, mucin aggregation is facilitated by the hydrophobic nonglycosylated patches,[22] promoting the formation of viscoelastic gels at a high mucin concentration (>14 mg/mL),[22] which contributes to hydrodynamic lubrication.[23] At biological surfaces, mucins facilitate boundary lubrication by their high hydration and by generating repulsive steric and electrostatic forces.[20] The lubrication properties of mucins on hydrophobic substrates have been studied by tribological measurements,[24] atomic force microscopy (AFM),[25] and surface force apparatus (SFA).[26]

Mucins are very important glycoprotein constituents of the tear fluid[3,27] and the ocular surface.[27] They contribute to the lubrication between corneal and conjunctival epithelial surfaces, aid water retention by acting as stabilizers of the preocular tear film, and serve as a barrier to prevent pathogen penetration.[4,28] Mucin deficiency and alternation in glycosylation characteristics can lead to dry eye syndrome.[4] Mucins can also adhere to contact lenses[29,30] and potentially modify the surface coating of the lenses, which may affect the comfort for the user.[4,31] Lord et al.[18] studied the adsorption of several tear film analogues *in vitro*, including mucin, onto different contact lens materials (PMMA and three hydroxyethyl methacrylate (p(HEMA)) based hydrogels) with quartz crystal microbalance with dissipation (QCM-D), and found that mucin adsorbed onto all of these surfaces. Hence, one can envisage the use of mucin in tear fluid substitutes to reduce dry eye related symptoms as well as contact lens discomfort (CLD) and improve the lubrication properties of contact lenses. In this work we elucidate interfacial properties of a recombinant mucin-type immunoglobulin fusion glycoprotein, PSGL-1/mIgG$_{2b}$, which is a brush-with-anchor-type mucin, as schematically shown in Figure 1. We compare the properties of this mucin with those of bovine submaxillary mucin (BSM), having an overall train-of-brushes structure as shown in Figure 1.

Adsorption of the two mucins to PMMA, a material commonly used in rigid gas permeable contact lenses, was determined using the QCM-D technique. We further elucidate the consequences of the adsorption in terms of lubrication properties of the mucin-coated PMMA surfaces, utilizing the AFM colloidal probe technique. This is the first report on friction properties of mucin layers adsorbed on PMMA surfaces. It is also the first study of interfacial properties of PSGL-1/mIgG$_{2b}$.

2. MATERIALS AND METHODS

2.1. Materials. BSM was purchased from Sigma (catalogue no. M3895) and used as received. The BSM has been reported to have a molecular weight of about 7×10^6 g/mol as determined by static light scattering.[32] Further, it contains 9–17% sialic acid residues ($pK_a \approx 2.6$) according to the manufacturer specifications. We note that commercial preparations of BSM also contain mucin-bound albumin, and that the presence of albumin has been noted to enhance the adsorption.[33,34] PSGL-1/mIgG$_{2b}$, provided by Recopharma, was used as received. The chrompure mouse IgG-Fc fragment was purchased from Jackson ImmunoResearch (Suffolk, U.K.; code no. 015-000-008; lot no. 107399) and used as received. This molecule, having two chains linked by disulfide bonds, has a molecular weight of around 50 kDa according to the manufacturer's specification. Sodium chloride (NaCl; BioXtra; ≥99.5%) was purchased from Sigma-Aldrich and used as received. Water was first pretreated with a Milli-RO 10 plus unit and further purified with a Milli-Q PLUS 185 system (Millipore). The resistivity of the water after the treatment was 18.2 MΩ cm, and the total organic carbon content of the water did not exceed 2 ppb. Mucin stock solutions of 200 ppm were prepared by dissolving weighted portions of mucin in 155 mM NaCl solution. All solutions were stored at 4 °C for at most 3 days and diluted with 155 mM NaCl solution prior to use. The pH of the NaCl, BSM, and PSGL-1/mIgG$_{2b}$ solutions was 5.8, 5.8, and 4.8, respectively.

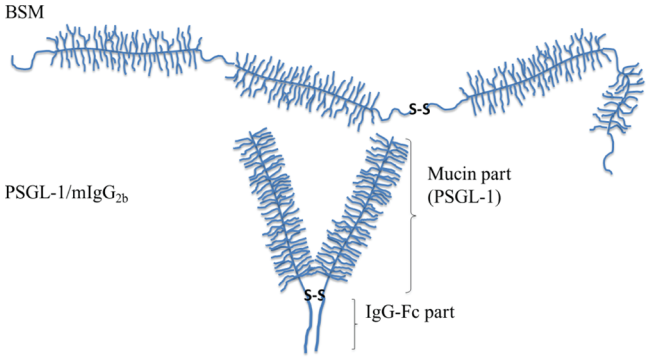

Figure 1. Schematic illustration of mucin structures (not drawn to scale). Top: secreted BSM consists of alternating nonglycosylated protein regions (thin line) and heavily glycosylated regions (with side chains). The overall structure can be characterized as a train-of-brushes. Bottom: PSGL-1/mIgG$_{2b}$ produced as a dimer containing two glycosylated brush regions attached to the Fc part of mIgG (the anchor block). The overall structure can be characterized as a brush-with-anchor. We note that the Fc part, as a dimer, contains two N-linked glycans (not shown in the sketch).

2.1.1. Recombinant Mucin, PSGL-1/mIgG$_{2b}$. PSGL-1/mIgG$_{2b}$ is a recombinant mucin-type fusion protein consisting of the extracellular part of P-selectin glycoprotein ligand-1 (PSGL-1) fused to the Fc part of mouse IgG$_{2b}$. PSGL-1/mIgG$_{2b}$ is mainly expressed as a dimer when produced in Chinese hamster ovary (CHO) cells, and the molecular weight is around 300 kDa.[35] PSGL-1/mIgG$_{2b}$ used in this study was produced in glycoengineered CHO cells coexpressing the core 2 *N*-acetylglycosyltransferase I (C2 GnT-I) and the α1,3-fucosyltransferase VII (FUT-VII). The production and characterization of PSGL-1/mIgG$_{2b}$ from these cells have been described previously.[36] PSGL-1 is a mucin-type glycoprotein expressed on the surface of myeloid cells. It is the high-affinity receptor for P-selectin which is expressed on activated endothelial cells and platelets. The interaction between PSGL-1 and its receptor P-selectin mediates tethering and rolling of leukocytes along the vascular endothelium at sites of inflammation. It is a membrane-bound protein with an extracellular domain rich in serines, threonines, and prolines. It has a highly extended structure with an extracellular domain

that is about 50 nm long,[37] and it has 53 potential *O*-glycosylation and three potential *N*-glycosylation sites.[38,39] Some key features of the two mucins used are summarized in Table 1.

Table 1. Selected Data for BSM and PSGL-1/mIgG$_{2b}$ Mucins

mucin	overall structure	molecular weight (kDa)	carbohydrate content (wt %)
BSM	train-of-brushes	7000	61−69
PSGL-1/mIgG$_{2b}$	brush-with-anchor	300	43 (ref 35)

2.1.2. Substrates. Poly(methyl methacrylate)-coated gold sensors (AT cut quartz crystals) with a diameter of 14 mm, QSX 999 (Q-sense, Västra Frölunda, Sweden), having a nominal resonance frequency of about 5 MHz, were used as the substrate for all experiments. The PMMA layer is spin-coated on the gold crystal surface and has a thickness of around 40 nm. The crystals were cleaned by rinsing with Milli-Q water and dried with a gentle flow of nitrogen gas before use. The water contact angle on the PMMA surface was determined to be 68°, as measured with a DataPhysics OCA40 micro (DataPhysics GmbH, Germany) instrument at 23 ± 0.5 °C and humidity of 44%.

2.2. Quartz Crystal Microbalance with Dissipation. A Q-sense E4 device (Q-sense) was employed for studying adsorption of mucins on PMMA surfaces. This device has the capacity to continuously measure the change in frequency and dissipation at the fundamental frequency as well as at six different overtone frequencies (15, 25, 35, 45, 55, and 65 MHz). In this work we utilized the third, fifth, and seventh overtones. A detailed description of the QCM-D technique has been provided by Rodahl et al.[40] The frequency change observed during adsorption (Δf) depends on the total mass added to the crystal, including solvent coupled to the adsorbed layer. Provided the adsorbed layer is thin, rigid, and homogeneous, the sensed mass is directly proportional to the frequency change according to the Sauerbrey equation.[41] However, in many cases the adsorbed layer is viscoelastic, and this requires more elaborate analysis models. The QCM-D device also measures dissipation changes (ΔD), which are energy losses in the adsorbed film. This allows a more accurate estimation of the sensed mass by using a viscoelastic model to analyze changes in both frequency and dissipation for several overtones, e.g., using the Voigt representation, which treats the viscoelastic response of the layer as that of a spring and a dashpot coupled in parallel. A detailed description of the viscoelastic model and discussions about its validity can be found elsewhere.[41] In our case we utilized the extended viscoelastic model.[42,43]

The extended viscoelastic model takes into account the frequency dependence of the viscoelastic properties of the adsorbed layer, and we utilized frequency and dissipation data from the third, fifth, and seventh overtones in the analysis. The modeling parameters used for analyzing the adsorption of PSGL-1/mIgG$_{2b}$ on PMMA are provided in the Supporting Information (Table S1).

2.3. Adsorption Procedure. All QCM-D experiments were started by obtaining a stable baseline in 155 mM NaCl solution. In the sequential adsorption experiments, 100 ppm BSM or PSGL-1/mIgG$_{2b}$ was injected into the cell. After the adsorption reached equilibrium, the system was rinsed by pumping 155 mM NaCl solution into the cell for 20 min. Next, the solution containing the other mucin type was injected into the cell and the response was followed until equilibrium was obtained. The surface was subsequently rinsed with 155 mM NaCl. In the stepwise adsorption experiments the surface was exposed to mucin solutions of increasing concentration (in 155 mM NaCl), and then the surface was rinsed with protein-free 155 mM NaCl. All experiments were performed at 25 ± 0.2 °C.

2.4. Atomic Force Microscope with Colloidal Probe. A Nanoscope Multimode III Pico Force atomic force microscope (AFM; Veeco Instruments Inc.) was employed for force and friction measurements performed in a fused silica liquid cell (volume ≈ 0.1 mL). Rectangular tipless cantilevers (Mikro-Masch, CSC12/tipless/Cr−Au) with the approximate dimensions of 250 μm in length, 35 μm in width, and normal spring constants in the range of 0.02−0.2 N/m were chosen for all force and friction measurements. The exact values of the normal (k_N) and the torsional (k_φ) spring constants were determined using the AFM Tune IT v2.5 software (Force IT, Järna, Sweden) adopting the method based on thermal noise with hydrodynamic damping.[44,45] A spherical PMMA particle (Kisker, catalog no. ppmma-10.0) with a diameter of approximately 10 μm was attached to the end of the cantilever with the aid of an Ependorf Micromanipulator 5171, a Nikon Optiphot 100S reflection microscope, and a small amount of epoxy glue (Araldite, 80806) after determining the spring constants of the cantilever. The lateral photodetector sensitivity (δ, V/rad) was calibrated using the method of tilting the AFM head proposed by Pettersson et al.[46]

The normal force curves were measured with a constant approach and retraction speed of 1 μm/s. In each case at least 10 curves were recorded. The force curves were then analyzed with the AFM Force IT software (Force IT). The deflection sensitivity obtained for the bare PMMA−PMMA system was used in all cases when defining the constant compliance region and generating force curves in the presence of adsorbed mucin layers. We note that zero separation is defined by the constant compliance region and does not provide any information on the layer thickness, which contrasts to measurements using a surface forces apparatus.[47] Friction forces were measured by capturing "contact mode images" using a scanning angle perpendicular to the cantilever at different applied loads at a sliding speed of 4 μm/s with a scan size of 2 μm. The frictional force values were recorded at the onset of the steric repulsion up to the hard wall region of the system and again on decreasing the load. The friction traces obtained were analyzed by employing the AFM Friction IT software (Friction IT).

2.5. Experimental Procedure of Normal and Friction Force Measurements. Before each experiment, the fused silica cell and all other tools were cleaned by immersion in 2% Hellmanex (Hellma GmbH) solution for 1 h and then rinsed excessively with Milli-Q water. They were then rinsed with ethanol before being dried with a stream of filtered nitrogen gas. The AFM experiments were started by measuring the normal forces between the PMMA surface and the PMMA colloidal probe across a 155 mM NaCl solution. This was followed by friction measurements. Next, a 100 ppm solution of mucin (BSM or PSGL-1/mIgG$_{2b}$) in 155 mM NaCl was introduced into the fused silica cell, and the polymer was allowed to adsorb for 45 min before measuring the surface forces again. After the force curves were recorded, friction measurement was performed, and then followed again by force measurements. This was done to check the stability of the

detector signal at zero load and to study if the friction measurements affected the mucin layers. After that, 155 mM NaCl solution was injected into the fused cell to replace the mucin solution. The same procedure (force−friction−force measurement) was repeated. All measurements were carried out at 25 °C.

3. RESULTS

3.1. Adsorption of Mucins on PMMA. Stepwise adsorption experiments were performed by injecting mucin solutions of increasing concentrations into the QCM cell, allowing the adsorption to proceed for 45 min at each concentration. The Voigt mass, i.e., the mass of the adsorbed mucin and water associated with the layer, after each adsorption step is provided in Figure 2. This data set should not be regarded as reflecting the adsorption isotherm since adsorption of mucin from dilute solutions occurs very slowly, and within the time frame of 45 min only the data point obtained at 100 ppm mucin concentration can be regarded as reflecting the equilibrium situation (as judged from the absence of further changes in frequency and dissipation at the end of the adsorption process).

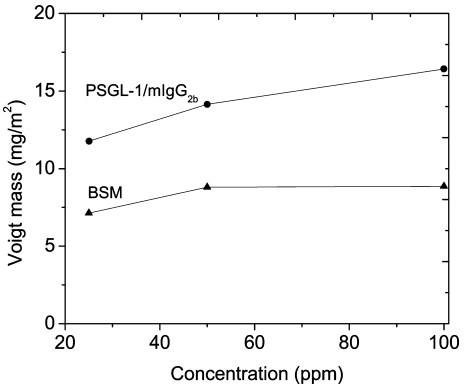

Figure 2. Voigt mass of BSM (triangles) and PSGL-1/mIgG$_{2b}$ (circles) as a function of the concentration of the respective mucin.

We note, however, that the Voigt mass of the PSGL-1/mIgG$_{2b}$ layer is significantly larger than that of the BSM layer. In the remainder of section 3.1 we first discuss the competitive adsorption of the two different types of mucin. Next, we address the adsorption of the PSGL-1/mIgG$_{2b}$ anchor block, the Fc fragment of mouse IgG. The QCM-D data also contain information related to the dynamics of layer formation, and this issue is also addressed.

3.1.1. Sequential Adsorption of BSM and PSGL-1/mIgG$_{2b}$. Two sequential adsorption experiments were performed to characterize the adsorption of BSM and PSGL-1/mIgG$_{2b}$ to PMMA. Figure 3a shows the data obtained when first adsorbing BSM to PMMA and then allowing PSGL-1/mIgG$_{2b}$ to interact with the BSM-coated surface.

The QCM-D response recorded during adsorption of BSM from 100 ppm solution was found to be quite complex. Initially a rapid decrease in frequency and increase in dissipation is observed as mass is added to the sensor surface during formation of a viscoelastic mucin layer. However, after about 10 min, the response of the sensor reverses and now the frequency slowly *increases* and the dissipation *decreases*. This indicates structural rearrangements leading to a less extended layer structure, as will be discussed further in section 3.1.3. The adsorption reached equilibrium within 2 h and only a limited amount of BSM was removed by rinsing. The frequency change resulting from the subsequent adsorption of PSGL-1/mIgG$_{2b}$ was around −25 Hz, and the dissipation of the composite BSM/PSGL-1/mIgG$_{2b}$ layer was higher than that of the initial BSM layer. Clearly, PSGL-1/mIgG$_{2b}$ can associate with the preadsorbed BSM layer, which increases the layer thickness (Table 2). It is also conceivable that some adsorbed BSM molecules are replaced by PSGL-1/mIgG$_{2b}$, even though this process requires penetration of the dimeric PSGL-1/mIgG$_{2b}$ through the preadsorbed BSM layer.

The QCM-D response due to adsorption of PSGL-1/mIgG$_{2b}$ on PMMA is less complex than that observed during BSM adsorption. In this case the frequency decreases and dissipation increases monotonically with time until equilibrium is reached as shown in Figure 3b. Exposure of this PSGL-1/mIgG$_{2b}$ layer to a BSM solution only results in minor changes in frequency and dissipation. Clearly, BSM cannot associate with the preadsorbed PSGL-1/mIgG$_{2b}$ layer (Figure 3b) whereas PSGL-1/mIgG$_{2b}$ does interact with preadsorbed layers of BSM (Figure 3a). This shows that the region of the PSGL-1/mIgG$_{2b}$ molecule that associates with BSM is buried within the preadsorbed PSGL-1/mIgG$_{2b}$ layer, and we suggest that it is the IgG Fc part of PSGL-1/mIgG$_{2b}$ that provides both the anchoring to PMMA and facilitates association with pre-

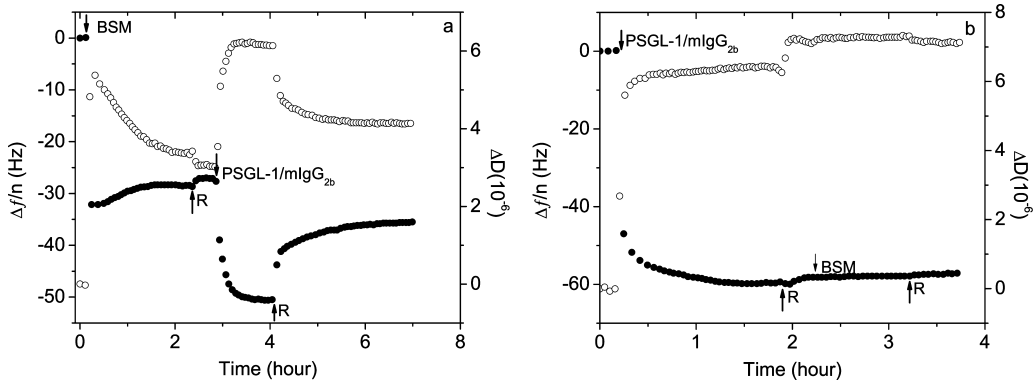

Figure 3. Frequency (filled circles) and dissipation (open circles) changes as a function of time during adsorption of an initial BSM layer followed by rinsing and PSGL-1/mIgG$_{2b}$ adsorption (a) and the reverse (b) (PSGL-1/mIgG$_{2b}$−rinsing−BSM adsorption). The concentration of all mucin solutions was 100 ppm in 155 mM NaCl. The arrows labeled with BSM and PSGL-1/mIgG$_{2b}$ mark the starting points of mucin injection, and the arrows labeled with "R" mark the starting point for rinsing with 155 mM NaCl solution.

Table 2. Characteristics of BSM and PSGL-1/mIgG$_{2b}$ Layers on PMMA Evaluated from Sequential Adsorption Experiments of the Type Shown in Figure 3

experiment 1: BSM followed by PSGL-1/mIgG$_{2b}$			experiment 2: PSGL-1/mIgG$_{2b}$ followed by BSM		
	Voigt thickness (nm)	Voigt mass (mg/m^2)		Voigt thickness (nm)	Voigt mass (mg/m^2)
BSM	7.3 ± 0.5	7.9 ± 0.5	PSGL-1/mIgG$_{2b}$	18.9 ± 0.2	20.4 ± 0.2
after rinsing	6.6 ± 0.5	7.2 ± 0.5	after rinsing	20.4 ± 0.2	22.0 ± 0.2
PSGL-1/mIgG$_{2b}$	13.2 ± 0.3	14.3 ± 0.3	BSM	20.5 ± 0.2	22.1 ± 0.2
after rinsing	9.8 ± 0.3	10.6 ± 0.3	after rinsing	20.1 ± 0.2	21.7 ± 0.2

adsorbed BSM, presumably via the nonglycosylated regions of BSM.

The Voigt mass of the two mucin layers formed from 100 ppm solutions is shown in Table 2 (data from sequential adsorption experiments as in Figure 3). It is striking that the Voigt mass and Voigt thickness of the PSGL-1/mIgG$_{2b}$ layer are more than 2 times higher than those of the BSM layer. We note that the Voigt mass of the BSM layer decreases after rinsing, which can be explained by a limited desorption. In contrast, the Voigt mass increases slightly for the PSGL-1/mIgG$_{2b}$ layer after rinsing, which is suggested to be due to the pH difference of the PSGL-1/mIgG$_{2b}$ mucin solution (pH 4.8) and the NaCl buffer solution (pH 5.8) that results in higher charge of PSGL-1/mIgG$_{2b}$ and increases the mass of water associated with the layer. The modeling results for the sequential adsorption experiments are summarized in Table 2. The standard deviation was calculated from three different experiments.

3.1.2. Adsorption of IgG-Fc to PMMA. To better understand the adsorption of PSGL-1/mIgG$_{2b}$ to PMMA, experiments were also carried out with the IgG-Fc part of PSGL-1/mIgG$_{2b}$, and the results are shown in Figure 4.

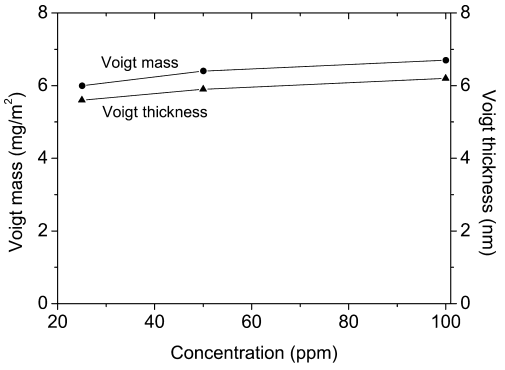

Figure 4. Voigt mass (circles) and thickness (triangles) of IgG-Fc on PMMA as a function of IgG-Fc concentration in 155 mM NaCl.

IgG-Fc adsorption on PMMA results in a Voigt mass of about 6 mg/m^2 at a concentration of 25 ppm (almost 3 h was required to reach equilibrium; see Figure S1 for the adsorption data and Figure S2 for the Voigt modeling result in the Supporting Information), increasing slightly to 6.5 mg/m^2 at 50 and 100 ppm IgG-Fc concentration. The corresponding Voigt layer thickness is around 5−6 nm. The weak dependence of the sensed mass on IgG-Fc bulk concentration is a sign of high surface affinity.[48] Thus, we conclude that the IgG-Fc fragment of PSGL-1/mIgG$_{2b}$ mucin contributes significantly to the anchoring of this mucin to PMMA.

3.1.3. ΔD vs Δf plots. The ΔD−Δf plots for adsorption of the two mucins and IgG-Fc on PMMA are shown in Figure 5. This type of plot can shed light on structural transitions

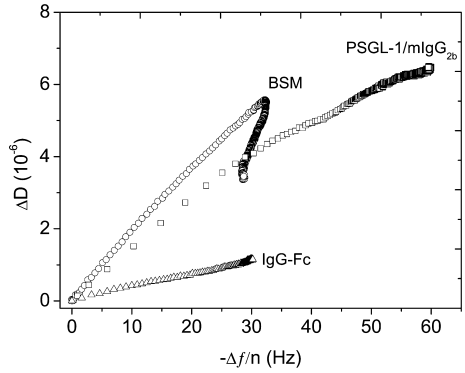

Figure 5. ΔD−Δf plot of BSM (circles), PSGL-1/mIgG$_{2b}$ (squares), and IgG-Fc (triangles) adsorbed on PMMA.

occurring as the adsorption proceeds. The ΔD−Δf curve for IgG-Fc is rather featureless and displays a linear relation between ΔD and Δf. In contrast, the ΔD−Δf curve for BSM consists of two regions, a first linear region up to 30 Hz and a second region with decreasing dissipation. This suggests that after the initial adsorption the adsorbed BSM molecules slowly change their conformation to form a thinner layer to maximize the favorable interaction with the surface.[49−51] The relatively small average Voigt thickness of the BSM layer, around 7 nm, suggests that most molecules are oriented parallel to the surface. This is also supported by the relatively small ΔD value compared to what is found for more extended polymer layers.[52]

The ΔD−Δf curve for PSGL-1/mIgG$_{2b}$ mucin is reminiscent of what has been observed for some synthetic bottle-brush polymers.[42,52] The first linear region (up to 30 Hz) suggests that initially most PSGL-1/mIgG$_{2b}$ molecules interact with the PMMA surface in a way similar to BSM, i.e., with the chains mainly parallel to the surface. The decreasing slope in the second region (30−45 Hz) means that the energy dissipated per unit sensed mass decreases, which signifies that the layer becomes stiffer due to increased interactions between adsorbed polymer chains, as also reported in other studies.[42,52] The increasing slope in the last region (>45 Hz) suggests a structural change toward a more extended layer conformation. This feature has also been observed for copolymers having one part that adsorbs stronger than the other and interpreted as expulsion of the block with less surface affinity from direct contact with the surface by the more strongly bound block.[42] We interpret our finding in a similar way and associate the block mediating strong adsorption with the IgG-Fc part of the PSGL-1/mIgG$_{2b}$.

3.2. Normal and Friction Forces. *3.2.1. Normal Forces between PMMA Surfaces.* The forces acting between two PMMA surfaces across 155 mM NaCl solution are shown in Figure 6. They are purely attractive except for the hard wall repulsion defining zero separation.

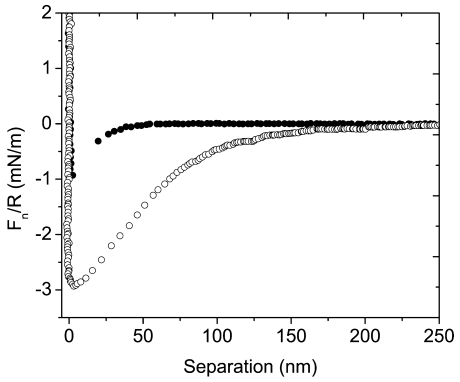

Figure 6. Force−separation curves (approach, filled circles; separation, open circles) between PMMA surfaces across 155 mM NaCl solution. The force is normalized by the particle radius. Note that the constant slope part of the force curves observed during jump-in and jump-out reflects the mechanical instability of the spring rather than the attractive surface forces.

On approach, the attractive force is noted once the separation has decreased to 40−50 nm, and it gives rise of an adhesion with a magnitude of around 3 mN/m. On separation, the attraction persists until the separation has increased to around 200 nm. The range of the attraction is larger than expected for a van der Waals force, as also has been observed for other polymeric surfaces such as polystyrene,[53,54] and interpreted as due to the presence of a few dangling chains or due to the presence of a few submicrometer airbubbles giving rise to a capillary attraction. We note that the exact range of the attraction and the adhesion (2−6 mN/m) varied somewhat between measurements, which could be expected by both of these mechanisms. Importantly, this attraction disappears when mucin is adsorbed. We also emphasize that the absence of any measurable electrostatic double-layer force does not mean that the surfaces must be uncharged, but it is a consequence of the high ionic strength (155 mM) that reduces the Debye-screening length to 0.8 nm and thus the range of any possible double-layer force accordingly.

3.2.2. Normal Forces between Mucin-Coated PMMA. The reproducibility of the forces measured between BSM- and PSGL-1/mIgG$_{2b}$-coated surfaces was found to be good, as shown in Figure S3 and Figure S4 in the Supporting Information. The force curves presented here were selected as one representative curves. The force curves measured after allowing BSM adsorption on the PMMA probe and PMMA surface for 45 min are shown in Figure 7a.

The forces experienced on approach are purely repulsive and of steric origin, i.e., due to compression of the BSM layer. On separation, a small but long-range attractive force is observed, which we assign to polymer bridging induced by BSM. The magnitude of the adhesion is reduced by about a factor of 10 compared to that observed before BSM adsorption. The presence of weak bridging attraction indicates that the surfaces are not fully covered by the adsorbed BSM molecules, as observed for other polymer-coated surfaces.[55]

The normal force curves recorded between PSGL-1/mIgG$_{2b}$-coated PMMA are shown in Figure 7b. A strong steric repulsion is observed on approach, and no or insignificant adhesion is noted on separation. The (close to) lack of adhesion between the PSGL-1/mIgG$_{2b}$ layers suggests a more complete coverage than that achieved for BSM, which is consistent with the QCM-D results. The hysteresis between trace and retrace force curves is small for PSGL-1/mIgG$_{2b}$ layers, indicating rapid recovery of the initial conformation as the force is released. This, in turn, suggests that no new and long-lived PSGL-1/mIgG$_{2b}$−surface bonds were formed due to compression. This can be understood if one part of the PSGL-1/mIgG$_{2b}$ molecule (the IgG-Fc part) is strongly anchored to the surface, whereas the other part (the glycosylated bottle-brush part) prefers contact with the bulk solution. The force curves determined after friction measurements, which are shown in the Supporting Information Figure S5 and Figure S6, do not show any significant differences compared to those reported in Figure 7. This demonstrates that the adsorbed mucin molecules are not removed by the combined action of shear and load.

The forces measured on approach between BSM-coated and PSGL-1/mIgG$_{2b}$-coated PMMA surfaces are compared in Figure 8, using a logarithmic force scale.

An exponential decay of the steric repulsion is observed at large separations as expected in the dilute tail region, where the repulsion mainly originates from the increase in osmotic pressure caused by the higher segment density between the surfaces compared to in bulk solution.[56] At further compression a more rapid increase in steric repulsion is expected and observed due to compression of the adsorbed polymer chains. A direct comparison of the magnitude of the steric repulsion in the two cases is not warranted since AFM colloidal probe force measurements, unlike measurements with the SFA,[57] do not

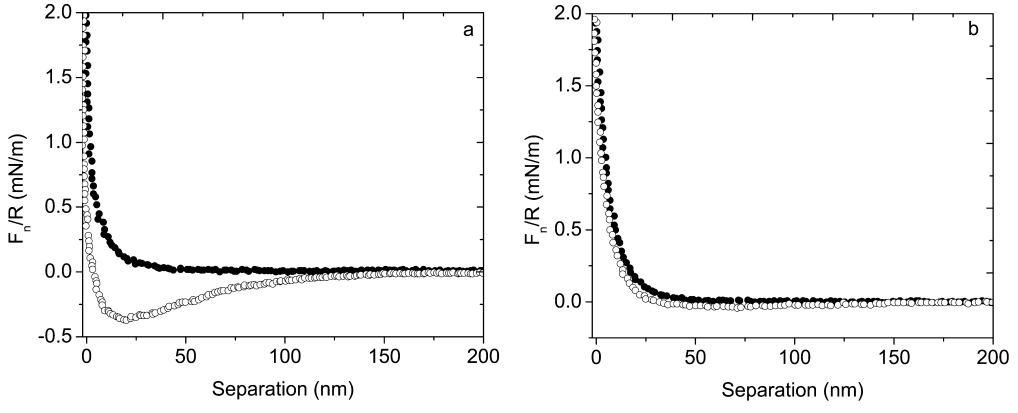

Figure 7. Force−separation curves (approach, filled circles; separation, open circles) between (a) BSM-coated PMMA and (b) PSGL-1/mIgG$_{2b}$-coated PMMA across 100 ppm solution of the respective mucin in 155 mM NaCl solution. The force is normalized by the particle radius.

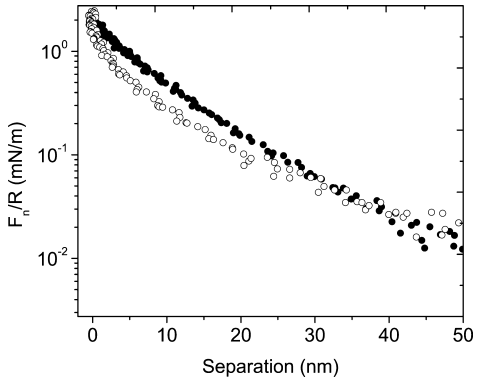

Figure 8. Force−separation curves measured on approach for BSM (open circles) and PSGL-1/mIgG$_{2b}$ (filled circles) on a logarithmic force scale. The mucin concentration was 100 ppm, and the NaCl concentration was 155 mM. The force is normalized by the particle radius.

provide direct information on the adsorbed layer thickness. However, from the QCM-D measurements we know that the PSGL-1/mIgG$_{2b}$ layer is significantly thicker than the BSM layer.

3.2.3. Friction Forces. The friction forces measured between PMMA surfaces across 155 mM NaCl were high, significantly smaller between BSM-coated PMMA, and even smaller between PSGL-1/mIgG$_{2b}$-coated PMMA, as illustrated in Figure 9a.

The friction vs load relationship can often be analyzed using the relation:[58]

$$F_f = C + \mu F_n \quad ([1])$$

where $C = S_C A$, with S_C being the critical shear stress and A the contact area.[58] The quantity C/μ is sometimes referred to as the dynamic adhesion[58] as it accounts for the adhesion between the surfaces during sliding motion, and μ is the friction coefficient. Since we only observed a significant adhesion between the bare PMMA surfaces, the critical shear stress has a nonzero value in only this case. The friction force and the friction coefficient between PMMA surfaces in 155 mM NaCl is very high, in line with what has been found for other nonpolar surfaces in water.[59] The friction coefficient, μ, equals 1.2 up to the highest load investigated. Thus the friction force law (nN) for the uncoated PMMA surfaces can be written as

$$F_f = 50 + 1.2F_n \quad ([2])$$

For BSM-coated PMMA surface the critical shear stress, and thus the dynamic adhesion, is close to zero and we recover the classical Amontons' rule, $F_f = \mu F_n$. The friction coefficient is found to be close to 0.7 up to the maximum load of 69 nN used in our experiment. Thus, in this case the friction force law is

$$F_f = 0.7F_n \quad ([3])$$

The friction versus load curve for PSGL-1/mIgG$_{2b}$ layers on PMMA is not linear (see Figure 9a), and in this case it is appropriate to define an effective friction coefficient, μ_{eff}, as

$$\mu_{eff} = \frac{F_f}{F_n} \quad ([4])$$

The effective friction coefficient as a function of load for PSGL-1/mIgG$_{2b}$-coated PMMA is shown in Figure 9b. We note that the effective friction coefficient is low, increasing from 0.02 at low loads to 0.24 at the highest load explored, 50 nN. Thus, it is clear that PSGL-1/mIgG$_{2b}$ layers provide superior lubrication of PMMA surfaces in aqueous environment compared to BSM.

When discussing friction data, it is sometimes better to report contact pressure than load, since the pressure values can be compared between experiments using probes with different radius and materials with different Young's moduli. We calculated the mean pressure that corresponds to a given load using Johnson, Kendall, Roberts (JKR) theory[60] for bare PMMA surfaces where the adhesion contribution is significant, and the Hertz model for PMMA surfaces coated with mucin layers where adhesion effects can be ignored.[61] The Young's modulus, 5 GPa,[62] and Poisson's ratio, 0.38, for PMMA were used in these calculations,[63] and the maximum forces applied to the mucin-coated surfaces correspond to a pressure of 8−9 MPa and at this point the flat contact area is about 6000 nm^2.

4. DISCUSSION

4.1. Adsorption of BSM on Nonpolar Surfaces. Adsorption of mucins to various surfaces has been extensively

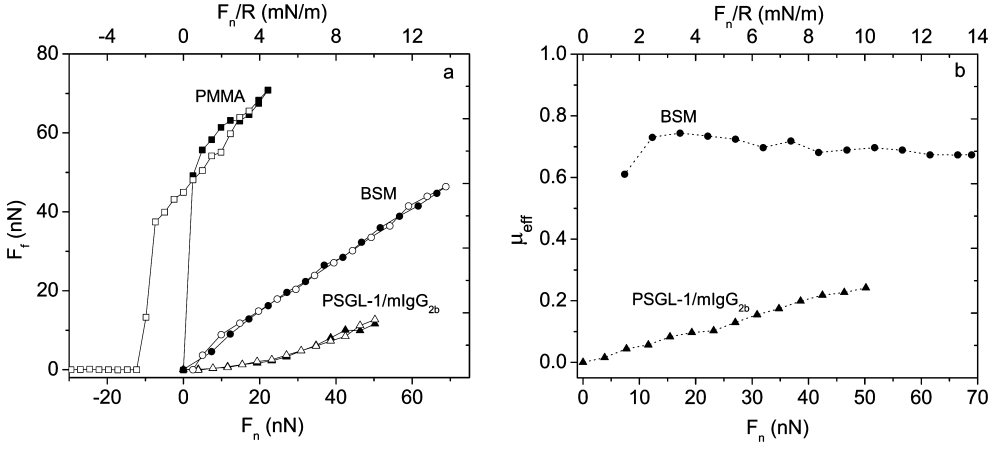

Figure 9. (a) Friction force, F_f, vs load, F_n and F_n/R, between two bare PMMA surfaces (squares) across 155 mM NaCl solution, BSM-coated PMMA (circles), and PSGL-1/mIgG$_{2b}$-coated PMMA layers (triangles) across 100 ppm mucin solutions in 155 mM NaCl. Filled and unfilled symbols represent data obtained on loading and unloading, respectively. (b) Effective friction coefficient, μ_{eff}, vs load for BSM (circles) and PSGL-1/mIgG$_{2b}$ (triangles).

dx.doi.org/10.1021/bm500173s | Biomacromolecules 2014, 15, 1515−1525

studied, and many results suggest that adsorption equilibrium is reached extremely slowly.[64] However, for BSM on PMMA we found that a plateau was obtained after 2 h when adsorption occurred from a 100 ppm solution in 155 mM NaCl, indicating that (close to) equilibrium had been reached.

The mass of the BSM layer, including trapped water, on PMMA was found to be 7.2 mg/m^2. This value is higher than what Lord et al. reported for BSM adsorbed from a 150 ppm solution on PMMA (5.1 ± 0.59 mg/m^2 including trapped water),[18] and what was found on hydrophobized silica (prepared by using chloro(dimethyl)octylsilane) where a sensed mass of about 5.9 mg/m^2 including water was obtained when BSM was adsorbed from a 200 ppm solution.[16]

The Voigt thickness of the BSM layer on PMMA found in this study is around 7 nm (see Table 2), which is in the range of other reported values on hydrophobic surfaces. For instance, Nikonenko et al. studied BSM adsorption from 1000 ppm solutions on PMMA with ellipsometry and reported a layer thickness of around 4 nm at different pH (3, 7, and 10) after 24 h adsorption time.[11] The thickness of the BSM layer on polystyrene particles, measured by flow-field-flow-fractionation and photon correlation spectroscopy, was reported to be 4−6 nm,[13] whereas Svensson et al. reported a thickness of 10 nm on hydrophobized silica as determined by ellipsometry.[17] Even though the thicknesses of BSM layers on partly hydrophobic surfaces vary somewhat depending on the nature of the substrate and the measurement technique, a value similar to the thickness of the backbone chain (estimated as 6 nm)[13] is obtained. Hence, it is clear that the majority of the material adsorbed is concentrated close to the surface, and that BSM has an orientation preferentially parallel to the surface. In fact, this orientation is, based on theoretical considerations, expected for charged polyelectrolytes adsorbed on uncharged surfaces.[65]

The fact that a relatively small thickness value is obtained from QCM-D and ellipsometric measurements does not preclude the presence of some long tails since these techniques are insensitive to the existence of a dilute tail region. Indeed, some authors have reported that some long tails are present for mucin layers on hydrophobic surfaces, and the adsorbed layer has been suggested to consist of an inner compact region with a thickness of 3−10 nm and an outer dilute tail region.[65,66] The data presented in this work are consistent with this view, where the compact inner region dominates the QCM-D response, whereas the dilute tail region results in a long-range steric force that clearly is observed in the surface force data (Figures 7 and 8).

The driving force for adsorption of mucins on hydrophobic surfaces has been suggested to be the entropic gain due to removal of water from contact with the hydrophobic surface and the nonglycosylated regions of the peptide backbone.[18] Our PMMA surface is weakly hydrophobic having a water contact angle ≈ 68° in agreement with literature values,[67] and it seems likely that the nonglycosylated regions of the BSM mucin backbone are preferentially adsorbed on the surface with the carbohydrate side chains extending toward solution.[7]

4.2. Adsorption of PSGL-1/mIgG$_{2b}$ on PMMA. Compared to BSM, PSGL-1/mIgG$_{2b}$ adsorbs significantly more to PMMA, and a more extended inner region of the layer is formed, as evidenced by the QCM-D data. The dilute tail region for BSM and PSGL-1/mIgG$_{2b}$ on PMMA surface does, on the other hand, appear to be rather similar as judged from the surface force curves (Figure 8). The more extended inner region of the layer for PSGL-1/mIgG$_{2b}$ is attributed to the strong affinity of the IgG-Fc part of this mucin that displaces the glycosylated region away from the surface, as also suggested by the $\Delta D-\Delta f$ plot (Figure 5).

4.3. Interactions between Adsorbed Mucin Layers on Nonpolar Surfaces. Interactions between mucin layers on hydrophilic surfaces have been studied extensively, but there are only a few reports on interactions between mucin-coated hydrophobic surfaces. Among these, Pettersson et al. studied BSM-coated mercaptohexadecane-modified gold surfaces with AFM[65] and found that long-range steric forces predominated the interaction due to the presence of some extended tails. They also noted a reduction in the repulsive steric force at high ionic strength due to screening of electrostatic forces between charged residues within the mucin molecule.[65] A reduction of the repulsion between porcine gastric mucin coated hydrophobized mica surfaces with increasing ionic strength was also observed by Harvey et al. Repulsion was obtained at separations below 100 nm between such mucin layers across pure water, but the onset of the repulsive force was reduced to about 40 nm across 0.1 M NaCl solution.[26] The interactions between rat gastric mucin (RGM) and pig gastric mucin (PGM) layers on hydrophobized mica were studied by Malmsten et al. using a surface force apparatus. Purely repulsive forces of steric origin were observed between RGM layers at separations below 150 nm. In contrast, an attraction on separation and more pronounced relaxation effects were found between PGM layers, which were explained in terms of slow relaxation, chain entanglement, and bridging.[66] We note that the different behavior of these two mucins is related to their different carbohydrate composition since their adsorbed amounts were similar.

Bridging was also found between BSM-coated hydrophilic mica surfaces by Perez and Proust, which was ascribed to low surface coverage and chain entanglement.[68] In fact, bridging is often observed between polymer-coated surfaces when the surface coverage is not too large.[17,69,70] We also propose bridging to be the origin of the small attraction observed on separation between BSM-coated PMMA surfaces in this study. In contrast, we do not note any significant attractive force between PSGL-1/mIgG$_{2b}$-coated PMMA surfaces. In this case, the higher layer mass and more extended layer structure (compared to BSM on PMMA surface) appear to effectively prevent bridging and chain entanglement.

4.4. Lubrication Ability of Mucin Layers on Nonpolar Surfaces. One of the many biological functions of mucins is to aid lubrication,[3] and one would thus expect mucin-coated surfaces to slide against each other with a low friction coefficient. However, in model experiments this is not always observed, but rather different results are reported in the literature even when the same mucin has been used. For instance, for BSM-coated silica surfaces Hahn-Berg et al.[71] reported a friction coefficient in the region of 0.2. In contrast, a much lower friction coefficient of 0.04 ± 0.02 was reported between a BSM-coated mica surface and a BSM-coated silica probe by Pettersson and Dėdinaitė,[25] and in this work we find a much higher friction coefficient of 0.7 between BSM-coated PMMA surfaces. To understand these very different results, we have to consider the main energy dissipative mechanisms between sliding polymer-coated surfaces.

First we note that the main energy dissipative mechanism and also the location of the shear plane may change with load. It has, for instance, been reported that the shear plane between two adsorbed polymer-coated surfaces at low loads was located

between the polymer layers but moved to the polymer−substrate interface at higher loads.[72] Klein has emphasized that a reduction in the interpenetration region between opposing polymer layers leads to lower friction,[21] and a small interpretation region is attained by densely packed polymer brush layers. Breakage and re-formation of polymer bridges, i.e., physical bonds between a polymer and two surfaces, also dissipates energy, and again densely packed layers counteract this energy dissipative process. A third energy dissipative mechanism arises from breakage and re-formation of physical segment−segment bonds, but this mechanism is expected to be low between mucin layers since water is a good solvent for the carbohydrate side chains. A fourth energy dissipative process arises from lateral motion of the adsorbed polymer along the surface due to the action of shearing. Strong surface−polymer affinity and energy barriers that prevent dragging of polymer chains along the surface counteract this process. These considerations suggest that the different results reported for BSM-coated surfaces are related to differences in the adsorbed amount and binding strength to the surface. Since the adsorbed amount of BSM to PMMA is not very low and bridging forces only give rise to a weak attraction on separation, we mean that bridging interactions cannot explain the high friction coefficient between BSM-coated PMMA surfaces. Instead we suggest that it arises from lateral movement of BSM, or regions of BSM, along the surface induced by shearing.

The low friction force for PSGL-1/mIgG$_{2b}$-coated PMMA surfaces is thus suggested to not only be related to the more extensive adsorption of PSGL-1/mIgG$_{2b}$ but also to its firmer anchoring to the PMMA surface via the IgG-Fc part. It is also expected that the degree of glycosylation and the type of carbohydrate residues present in the mucin molecules will affect lubrication. To investigate this requires access to mucins with the same anchoring group but different carbohydrate compositions. Such studies can be made possible by the recombinant approach used to build the PSGL-1/mIgG$_{2b}$ mucin used in this study.[36,39]

Another lubrication study between mucin-coated hydrophobized mica surfaces was reported recently by Harvey et al., using a surface force balance. They achieved a friction coefficient as low as 0.01−0.02 (up to 0.7 MPa), using a porcine gastric mucin ("Orthana" mucin).[26] This Orthana mucin has a dumbbell-like structure, with two globular nonglycosylated sections linked by a heavily glycosylated spacer. Presumably these nonglycosylated regions anchor the mucin to the hydrophobic surface, just like the IgG-Fc part of PSGL-1/mIgG$_{2b}$.

The friction coefficient of various contact lenses was measured by Roba et al. with a microtribometer at a contact pressure of 2.7−6.7 kPa, and the value was reported to be in the range of 0.02−0.34 for daily disposable contact lenses and 0.01−0.56 for reusable contact lenses in their operating environment.[73] The normal range of intraocular pressure (IOP, the tissue pressure of the intraocular contents) is 10−20 mmHg (≈1−3 kPa), corresponding to a force of only 1×10^{-9} nN in our experimental setup, and it is maintained at this level throughout life.[74] This pressure is much lower than the maximum pressure explored in this study. We mean that the low friction force and effective friction coefficient found between PSGL-1/mIgG$_{2b}$-coated PMMA surfaces at low loads, see Figure 9, suggests that such mucin coatings are appropriate for contact lens applications.

5. CONCLUSION

Interfacial properties of a train-of-brushes-type mucin, BSM, and a brush-with-anchor-type mucin, PSGL-1/mIgG$_{2b}$, on PMMA in contact with 155 mM NaCl solution have been investigated using QCM-D and surface force and friction measurements. We find large differences between these two types of mucins. The PSGL-1/mIgG$_{2b}$ mucin layer has a significantly larger mass than the BSM layer (including water in the layer), and the inner region of this layer is more extended than that for BSM as deduced from the QCM-D measurements. Both layers also contain an outer dilute tail region, which generates a long-range steric repulsion that is rather similar for the two types of mucins.

The IgG-Fc anchor block of the PSGL-1/mIgG$_{2b}$ mucin appears to replace the oligosaccharide rich domains in PSGL-1/mIgG$_{2b}$ at the PMMA surface at the later stage of the adsorption process, as judged from the ΔD vs Δf plot.

The recombinant PSGL-1/mIgG$_{2b}$ mucin is found to be a superior boundary lubricant on PMMA compared to BSM up to pressures in the 8−9 MPa regime. We argue that this is a consequence of the higher layer mass for PSGL-1/mIgG$_{2b}$ and the higher surface affinity provided by the IgG-Fc anchor block, which counteracts bridging and lateral motion of molecules along the surface during shearing. The favorable boundary lubrication properties of PSGL-1/mIgG$_{2b}$ layers were found even though the layers were formed by adsorption from dilute solution (100 ppm) within a short adsorption time (45 min), which is promising for the use of this mucin as coatings on nonpolar materials such as PMMA.

■ ASSOCIATED CONTENT

Supporting Information

Table listing Voigt modeling parameter settings, figures showing adsorption of IgG-Fc to PMMA surface obtained by QCM-D, reproducibility of the force curves measured between mucin-coated surfaces, and comparison between force curves measured before and after friction measurements, and text decribing additional parameters and results as well as accompanying references. This material is available free of charge via the Internet at http://pubs.acs.org.

■ AUTHOR INFORMATION

Corresponding Author

*E-mail: andra@kth.se.

Notes

The authors declare the following competing financial interest(s): J.H. is a part time CEO/CSO, board member and shareholder of Recopharma AB.

■ ACKNOWLEDGMENTS

P.M.C. and J.A. acknowledge financial support from the Swedish Research Council (VR). A.D. acknowledges support from VINNOVA. J.A. thanks Esben Thormann and Chao Liu for introducing her to AFM colloidal probe measurements.

■ REFERENCES

(1) Bansil, R.; Turner, B. S. *Curr. Opin. Colloid Interface Sci.* **2006**, *11*, 164−170.

(2) Strous, G.; Dekker, J. *Crit. Rev. Biochem. Mol. Biol.* **1992**, *27*, 57−92.

(3) Davidson, H. J.; Kuonen, V. J. *Vet. Ophthalmol.* **2004**, *7*, 71−77.

(4) Ramamoorthy, P.; Nichols, J. J. *Optom. Vision Sci.* **2008**, *85*, 631−642.
(5) Cárdenas, M.; Elofsson, U.; Lindh, L. *Biomacromolecules* **2007**, *8*, 1149−1156.
(6) Shi, L. *Trends Glycosci. Glycotechnol.* **2000**, *12*, 229−239.
(7) Shi, L.; Ardehali, R.; Caldwell, K. D.; Valint, P. *Colloids Surf., B* **2000**, *17*, 229−239.
(8) Bansil, R.; Stanley, E.; Lamont, J. T. *Annu. Rev. Physiol.* **1995**, *57*, 635−657.
(9) Znamenskaya, Y.; Sotres, J.; Engblom, J.; Arnebrant, T.; Kocherbitov, V. *J. Phys. Chem. B* **2012**, *116*, 5047−5055.
(10) Harding, S. E. *Adv. Carbohydr. Chem. Biochem.* **1989**, *47*, 345−381.
(11) Nikonenko, N. A.; Bushnak, I. A.; Keddie, J. L. *Appl. Spectrosc.* **2009**, *63*, 889−898.
(12) Patel, M. M.; Smart, J. D.; Nevell, T. G.; Ewen, R. J.; Eaton, P. J.; Tsibouklis, J. *Biomacromolecules* **2003**, *4*, 1184−1190.
(13) Shi, L.; Caldwell, K. D. *J. Colloid Interface Sci.* **2000**, *224*, 372−381.
(14) Feldoto, Z.; Pettersson, T.; Dėdinaitė, A. *Langmuir* **2008**, *24*, 3348−3357.
(15) Feiler, A. A.; Sahlholm, A.; Sandberg, T.; Caldwell, K. D. *J. Colloid Interface Sci.* **2007**, *315*, 475−481.
(16) Halthur, T. J.; Arnebrant, T.; Macakova, L.; Feiler, A. *Langmuir* **2010**, *26*, 4901−4908.
(17) Svensson, O.; Lindh, L.; Cárdenas, M.; Arnebrant, T. *J. Colloid Interface Sci.* **2006**, *299*, 608−616.
(18) Lord, M. S.; Stenzel, M. H.; Simmons, A.; Milthorpe, B. K. *Biomaterials* **2006**, *27*, 567−575.
(19) Svensson, O.; Arnebrant, T. *Curr. Opin. Colloid Interface Sci.* **2010**, *15*, 395−405.
(20) Coles, J. M.; Chang, D. P.; Zauscher, S. *Curr. Opin. Colloid Interface Sci.* **2010**, *15*, 406−416.
(21) Raviv, U.; Giasson, S.; Kampf, N.; Gohy, J.-F.; Jérôme, R.; Klein, J. *Nature* **2003**, *425*, 163−165.
(22) Bromberg, L. E.; Barr, D. P. *Biomacromolecules* **2000**, *1*, 325−334.
(23) Yakubov, G. E.; Papagiannopoulos, A.; Rat, E.; Easton, R. L.; Waigh, T. A. *Biomacromolecules* **2007**, *8*, 3467−3477.
(24) Yakubov, G. E.; McColl, J.; Bongaerts, J. H. H.; Ramsden, J. J. *Langmuir* **2009**, *25*, 2313−2321.
(25) Pettersson, T.; Dėdinaitė, A. *J. Colloid Interface Sci.* **2008**, *324*, 246−256.
(26) Harvey, N. M.; Yakubov, G. E.; Stokes, J. R.; Klein, J. *Biomacromolecules* **2011**, *12*, 1041−1050.
(27) Argüeso, P.; Gipson, I. K. *Exp. Eye Res.* **2001**, *73*, 281−289.
(28) Gipson, I. K. *Exp. Eye Res.* **2004**, *78*, 379−388.
(29) Allansmith, M. R.; Korb, D.; Greiner, J. V.; Henriquez, A. S.; Simon, M. A.; Finnemore, V. M. *Am. J. Ophthalmol.* **1977**, *83*, 697−708.
(30) Fowler, S. A.; Greiner, J. V.; Allansmith, M. R. *Am. J. Ophthalmol.* **1979**, *88*, 1056−1061.
(31) Berry, M.; Harris, A.; Corfield, A. P. *Invest. Ophthalmol. Visual Sci.* **2003**, *44*, 567−572.
(32) Bastardo, L.; Claesson, P.; Brown, W. *Langmuir* **2002**, *18*, 3848−3853.
(33) Sandberg, T.; Blom, H.; Caldwell, K. D. *J. Biomed. Mater. Res., Part A* **2009**, *91A*, 762−772.
(34) Lundin, M.; Sandberg, T.; Caldwell, K. D.; Blomberg, E. *J. Colloid Interface Sci.* **2009**, *336*, 30−39.
(35) Liu, J.; Weintraub, A.; Holgersson, J. *Xenotransplantation* **2003**, *10*, 149−163.
(36) Gaunitz, S.; Liu, J.; Nilsson, A.; Karlsson, N.; Holgersson, J. *Glycoconjugate J.* **2014**, *31*, 145−159.
(37) Li, F.; Erickson, H. P.; James, J. A.; Moore, K. L.; Cummings, R. D.; McEver, R. P. *J. Biol. Chem.* **1996**, *271*, 6342−6348.
(38) Sako, D.; Chang, X.-J.; Barone, K. M.; Vachino, G.; White, H. M.; Shaw, G.; Veldman, G. M.; Bean, K. M.; Ahern, T. J.; Furie, B.; Cumming, D. A.; Larsen, G. R. *Cell* **1993**, *75*, 1179−1186.
(39) Nilsson, A.; Holgersson, J. *Expert Opin. Drug Discovery* **2006**, *1*, 161−178.
(40) Rodahl, M.; Höök, F.; Krozer, A.; Brzezinski, P.; Kasemo, B. *Rev. Sci. Instrum.* **1995**, *66*, 3924.
(41) Voinova, M. V.; Rodahl, M.; Jonson, M.; Kasemo, B. *Phys. Scr.* **1999**, *59*, 391.
(42) Iruthayaraj, J.; Olanya, G.; Claesson, P. M. *J. Phys. Chem. C* **2008**, *112*, 15028−15036.
(43) Dunér, G.; Thormann, E.; Dėdinaitė, A. *J. Colloid Interface Sci.* **2013**, *408*, 229−234.
(44) Green, C. P.; Lioe, H.; Cleveland, J. P.; Prokch, R.; Mulvaney, P.; Sader, J. E. *Rev. Sci. Instrum.* **2004**, *75*, 1988.
(45) Sader, J. E.; Chon, J. W. M.; Mulvaney, P. *Rev. Sci. Instrum.* **1999**, *70*, 3967.
(46) Pettersson, T.; Nordgen, N.; Rutland, M. W.; Feiler, A. A. *Rev. Sci. Instrum.* **2007**, 093702.
(47) Raviv, U.; Klein, J. *Science* **2002**, *297*, 1540−1543.
(48) Fleer, G.; Stuart, M. A. C.; Scheutjens, J. M. H. M.; Cosgrove, T.; Vincent, B. *Polymers at interfaces*; Chapman & Hall: London, U.K., 1993; pp 265−271.
(49) Sethuraman, A.; Vedantham, G.; Imoto, T.; Przybycien, T.; Belfort, G. *Proteins: Struct., Funct., Bioinf.* **2004**, *56*, 669−678.
(50) Ishiguro, R.; Yokoyama, Y.; Maeda, H.; Shimamura, A.; Kameyama, K.; Hiramatsu, K. *J. Colloid Interface Sci.* **2005**, *290*, 91−101.
(51) Martin, A. H.; Meinders, M. B. J.; Bos, M. A.; Cohen Stuart, M. A.; van Vliet, T. *Langmuir* **2003**, *19*, 2922−2928.
(52) Liu, X.; Dedinaite, A.; Rutland, M.; Thormann, E.; Visnevskij, C.; Makuska, R.; Claesson, P. M. *Langmuir* **2012**, *28*, 15537−15547.
(53) Vinogradova, O. I.; Yakubov, G. E.; Butt, H.-J. *J. Chem. Phys.* **2001**, *114*, 8124−8131.
(54) Thormann, E.; Simonsen, A. C.; Hansen, P. L.; Mouritsen, O. G. *Langmuir* **2008**, *24*, 7278−7284.
(55) Klein, J.; Luckham, P. F. *Nature* **1984**, *308*, 836−837.
(56) Israelachvili, J. N. In *Intermolecular and Surface Forces*, 3rd ed.; Israelachvili, J. N., Ed.; Academic Press: San Diego, CA, USA, 2011; pp 381−413.
(57) Claesson, P. M.; Ederth, T.; Bergeron, V.; Rutland, M. W. *Adv. Colloid Interface Sci.* **1996**, *67*, 119−183.
(58) Álvarez-Asencio, R.; Pan, J.; Thormann, E.; Rutland, M. W. *Tribol. Lett.* **2013**, *50*, 387−395.
(59) Hansson, P. M.; Claesson, P. M.; Swerin, A.; Briscoe, W. H.; Schoelkopf, J.; Gane, P. A. C.; Thormann, E. *Phys. Chem. Chem. Phys.* **2013**, *15*, 17893−17902.
(60) Johnson, K. L.; Kendall, K.; Roberts, A. D. *Proc. R. Soc. London, Ser. A* **1971**, *324*, 301−313.
(61) Hertz, H. *J. Reine Angew Math.* **1881**, *92*, 156−171.
(62) Wei, G.; Bhushan, B.; Ferrell, N.; Hansford, D. *J. Vac. Sci. Technol., A* **2005**, *23*, 811−819.
(63) Bhushan, B.; Burton, Z. *Nanotechnology* **2005**, *16*, 467−478.
(64) Dédinaité, A. *Encyclopedia of Surface and Colloid Science*, 2nd ed.; Taylor & Francis: New York, NY, USA, 2007; pp 1−17.
(65) Pettersson, T.; Feldötö, Z.; Claesson, P. M.; Dedinaite, A. In *Surface and Interfacial Forces—From Fundamentals to Applications*; Auernhammer, G., Butt, H.-J., Vollmer, D., Eds.; Springer: Berlin, Heidelberg: 2008; Vol. *134*, pp 1−10.
(66) Malmsten, M.; Blomberg, E.; Claesson, P.; Carlstedt, I.; Ljusegren, I. *J. Colloid Interface Sci.* **1992**, *151*, 579−590.
(67) Ma, Y.; Cao, X.; Feng, X.; Ma, Y.; Zou, H. *Polymer* **2007**, *48*, 7455−7460.
(68) Perez, E.; Proust, J. E. *J. Colloid Interface Sci.* **1986**, *118*, 182−191.
(69) Kampf, N.; Raviv, U.; Klein, J. *Macromolecules* **2004**, *37*, 1134−1142.
(70) Liu, X.; Thormann, E.; Dedinaite, A.; Rutland, M.; Visnevskij, C.; Makuska, R.; Claesson, P. M. *Soft Matter* **2013**, *9*, 5361−5371.
(71) Hahn Berg, I. C.; Lindh, L.; Arnebrant, T. *Biofouling* **2004**, *20*, 65−70.

(72) Klein, J.; Kumacheva, E.; Perahia, D.; Fetters, L. J. *Acta Polym.* **1998**, *49*, 617−625.
(73) Roba, M.; Duncan, E. G.; Hill, G. A.; Spencer, N. D.; Tosatti, S. G. P. *Tribol. Lett.* **2011**, *44*, 387−397.
(74) Murgatroyd, H.; Bembridge, J. *Contin. Educ. Anaesth., Crit. Care Pain* **2008**, *8*, 100−103.